Journal of Materials Chemistry B

RSC Publishing

PAPER

View Article Online
View Journal | View Issue

A pH sensitive ratiometric fluorophore and its application for monitoring the intracellular and extracellular pHs simultaneously†

Cite this: *J. Mater. Chem. B*, 2013, **1**, 661

Jin Zhou,[ab] Canliang Fang,[ab] Tianjun Chang,[ab] Xiangjun Liu[a] and Dihua Shangguan*[a]

Received 28th September 2012
Accepted 13th November 2012

DOI: 10.1039/c2tb00179a

www.rsc.org/MaterialsB

Intracellular and extracellular pH plays a key role in many cell biological processes. Probes for simultaneously monitoring the pH change inside and outside living cells are rarely available. In this paper, we describe a new ratiometric pH fluorophore that was synthesized by condensation of 4-bromine-1,8-naphthalimides and 3-amino-1,2,4-triazole. In the range of pH 5–8, the only N–H in the heterocycle-fused aromatic ring system of this fluorophore undergoes a reversible deprotonation–protonation process, which results in a large red shift of the absorption and emission spectra. In aqueous solution, this fluorophore exhibits good pH selectivity, high photostability, high tolerance to ionic strength, and high fluorescence quantum yield in both the acid and base forms. A long chain derivative of this fluorophore (HNNA) was designed for cellular pH sensing. HNNA was found to locate on the membrane structure of the cells, and was successfully used for mapping the pH change in both the extracellular microenvironment and the inner cells by confocal imaging.

Introduction

It is well known that intracellular and extracellular pH plays a key role in many physiological and pathological processes.[1] Extracellular pH is known to become lower in tumor microenvironments[2] and in several other physiological events.[3] Sensors that can reveal the pH difference between the intracellular and extracellular regions would be helpful for studies of cancer and cell biology.[4] However, very few pH sensors reported so far can simultaneously monitor the intracellular and extracellular pH in biological environments.

Fluorescence-based pH sensors are very powerful tools for monitoring pH change in biological samples. However, most of the current pH sensors respond to pH change by increasing or decreasing the fluorescence intensity; this single-intensity-based sensing is usually compromised by many non-pH factors, such as concentration changes of the probes, the drift of the light source or detector, as well as environmental effects in complex samples. A ratiometric fluorescent probe can avoid these problems by measuring the ratio of the emission intensities at two different wavelengths, which has attracted intense research efforts recently.[5]

The widely used small molecule indicators for intracellular pH are pyrene dyes and xanthene dyes.[6] However, some problems of these dyes, such as fast leakage, lack of membrane permeability, poor photostability or sensitivity to ionic strength, have to be considered in practical applications.[1] To overcome these problems, some ratiometric pH sensors based on nanoscaffolds have been designed; their fluorescent signal ratio arises from a pH-sensitive dye and a pH-insensitive reference dye, as well as fluorescence resonance energy transfer (FRET).[7] However, the cytotoxicity and the uncertain cellular location of nanoparticles limit the application of these pH sensors in living cells. Therefore, new small molecules for ratiometric pH measurement are still necessary. Recently a ratiometric, near-infrared fluorescent pH probe has shown good potential for intracellular pH sensing which is based on aminocyanine bearing a diamine moiety.[8] The pH change only causes the shift of the excitation spectrum of this probe, resulting in the changes of the fluorescence ratio excited at different wavelengths. Additionally, the fluorescence quantum yield of cyanine dyes is low.

An ideal ratiometric pH probe should exhibit shifted absorption or emission spectra upon pH change, its fluorescence quantum yields should be high in both acidic and basic states, moreover, the change of absorption or emission spectra should be reversible. For pH imaging in cells, this probe should have good membrane permeability, clear cellular location and low cytotoxicity. Herein, we report a novel pH-sensitive fluorophore, 3-amino-1,2,4-triazole fused 1,8-naphthalimide (Scheme 1), which exhibits ratiometric fluorescent response to pH change in physiological range. A long-chain derivative of

[a]*Beijing National Laboratory for Molecular Sciences, Key Laboratory of Analytical Chemistry for Living Biosystems, Institute of Chemistry, Chinese Academy of Sciences, Beijing, 100190, China. E-mail: sgdh@iccas.ac.cn*

[b]*Graduate School of the Chinese Academy of Sciences, Beijing 100049, China*

† Electronic supplementary information (ESI) available. See DOI: 10.1039/c2tb00179a

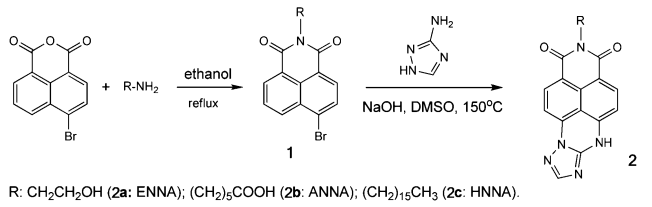

Scheme 1 Synthetic processes for the pH probes.

this fluorophore (HNNA) was designed and successfully applied to monitor the pH change in the intracellular and extracellular microenvironments. This is the first time it has been reported that a new naphthalimide derivative can simultaneously monitor intracellular and extracellular pH by the ratio response.

Results and discussion

Synthesis

4-Aminonaphthalimide derivatives have high fluorescence quantum yield, large Stoke's shift, good photostability, and were widely used for the design of fluorescent probes.[9] Some fluorescent pH sensors based on naphthalimide have been reported,[10] but none of them exhibit ratiometric fluorescence response. The new pH-sensitive fluorophore was synthesized by condensation of 4-bromine-1,8-naphthalimides and 3-amino-1,2,4-triazole (Scheme 1). The 4-bromine-1,8-naphthalimides were prepared from 4-bromine-1,8-naphthalic anhydride and primary amines. The final products were 3-amino-1,2,4-triazole fused naphthalimides; the fused ring structure was confirmed by NMR spectra (DEPT-135°, ^{1}H,^{1}H-COSY, HSQC and NOSEY), and high-resolution mass spectrometry (see Supporting Information for details†).

pH responses of ENNA

An *N*-hydroxyethyl derivative, ENNA (**2a**) exhibited good solubility in aqueous solution, and showed a colour change from yellow to dark orange (Fig. 1b) and a fluorescence change from light blue to green (Fig. 1d) with the pH increase from 5.0–8.0. Therefore ENNA was used for investigation of the optical properties of this pH-sensitive fluorophore. The pH-dependent absorbance spectra (Fig. 1a) of ENNA show a 40 nm red-shift from acidic state to basic state. Two isoabsorptive points at 395 nm and 455 nm indicate that two distinct chromophores are present at equilibrium. The absorbance ratio at 480 nm and 440 nm (A_{480nm}/A_{440nm}) (Fig. 1b) shows a significant pH response in the range of 5.0–8.0. The emission spectra of ENNA (Fig. 1c) under excitation at the isoabsorptive point (455 nm) show a 30 nm red-shift from acidic state to basic state. The ratiometric fluorescence intensity at 480 and 510 nm (I_{480nm}/I_{510nm}) (Fig. 1d) also shows a good pH response in the range of 5.0–7.5.

An *N*-carboxyhexyl derivative, ANNA (**2b**) showed almost identical optical properties to ENNA (see Fig. S1 and 2†), indicating that the optical response of both molecules to pH change comes from the heterocycle-fused aromatic ring system and is not affected by the substituent at the imide N-atom.

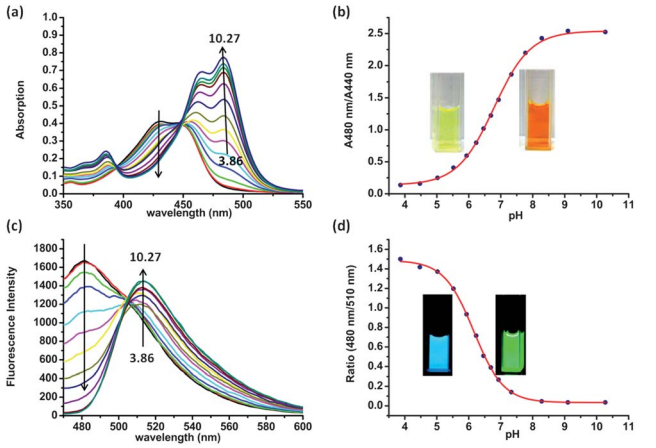

Fig. 1 (a) Absorption spectra of 50 μM ENNA; all samples were measured in HEPES buffer at pH 3.86, 4.47, 5.02, 5.52, 5.93, 6.23, 6.46, 6.69, 6.93, 7.33, 7.77, 8.28, 9.10, and 10.27. (b) Response curve of ratiometric absorbance (A_{480nm}/A_{440nm}) to pH. (c) Fluorescence spectra of 1.0 μM ENNA. All samples were measured in 20 mM HEPES buffer at pH 3.86, 4.47, 5.02, 5.52, 5.93, 6.23, 6.46, 6.69, 6.93, 7.33, 7.77, 8.28, 9.10, and 10.27. (d) Response curve of ratiometric fluorescence intensity (I_{480nm}/I_{510nm}, λ_{ex} = 455 nm) to pH.

Furthermore, the fluorescence changes of ENNA and ANNA were found to be reversible with the change of pH (see Fig. S3, ESI†), suggesting that our probes are stable towards the pH change. The significant changes of both absorbance and emission spectra with the pH change in the physiological range indicate that the 3-amino-1,2,4-triazole fused naphthalimide can serve as a fluorophore for colorimetric and fluorescent ratiometric pH measurements. This fluorophore combines the advantages of the sensitivity of fluorescence with the convenience and aesthetic appeal of a visual assay.

Salt concentration has been reported to influence the absorbance and emission spectra of highly charged pH indicators. The pK_as of these dyes are dependent on the ionic strength of the buffer.[11] To examine the effect of ionic strength on the optical properties of ENNA, pH titration experiments were performed in HEPES buffer containing different concentrations of NaCl (0, 100, 150, 200 mM) (see Fig. S4 and 5, ESI†), as well as in PBS buffer plus NaCl (0, 100, 150, 200 mM) (see Fig. S6 and 7, ESI†). The emission spectra and the ratio of emission intensity at 480 and 510 nm (I_{480nm}/I_{510nm}) were almost not influenced by the change of ionic strength. The negligible cross-sensitivity towards ionic strength may be due to the low number of charges of ENNA. These results suggest that this fluorophore is applicable to physiological ionic strength.

The ground-state pK_as of ENNA and ANNA were determined to be 6.53 ± 0.03 and 6.44 ± 0.03 by absorption titration in HEPES buffer (containing 150 mM NaCl) (see Fig. S8, ESI†). Both pK_a values are within the physiological pH range, suggesting that this fluorophore could serve as a pH probe for use in biological samples. The fluorescence quantum yield (Φ_f) of ENNA was determined by using *N*-butyl-4-butylamine-1,8-naphthalimide (Φ_f = 0.7 in ethanol) as the standard.[12] In HEPES buffer at pH 7.44, the fluorescence emission maximum of the deprotonated ENNA species is located at 510 nm with Φ_f = 0.49. In HEPES buffer at pH 4.20, the emission maximum of ENNA

lies at 480 nm with $\Phi_f = 0.95$ (Ex: 430 nm; Em: 440–700 nm). The high Φ_f in both acid and base forms in aqueous solution may be attributed to the large conjugated planar structure of this fluorophore. Compared with in the acid form, the relatively lower Φ_f in the base form might be attributed to the enhanced non-radiative decay resulted from the increased interaction of the anion form and water or counter ions in solution. The high Φ_f of ENNA in both states indicates that this fluorophore can serve as a good ratiometric fluorescent probe for pH measurement.

Mechanism of the pH response of ENNA

The visible colour and strong fluorescence of 4-aminonaphthalimide derivatives are due to their outstanding internal charge transfer (ICT) from the electron-rich amino group to the electron-poor imide moiety.[9] The above optical properties of ENNA can also be attributed to the ICT mechanism (Fig. 2a). The mechanism of the pH response of ENNA was investigated by ^{1}H NMR spectroscopy. Compared to the ^{1}H NMR spectra of ENNA in acidic state (LH), the N–H signal (peak e) of ENNA in basic state (L^-) disappeared (Fig. 2b), which suggests the deprotonation of N–H (Fig. 2a). The electrospray ionization-mass spectrometry (ESI-MS) analysis in negative ion mode only exhibited a prominent peak at m/z 320.1 (Fig. S9†), corresponding to the $(M - H)^-$ of ENNA, and no $(M + H)^+$, $(M + Na)^+$ or $(M + K)^+$ ion peaks were found in positive ion mode, suggesting that ENNA can be deprotonated easily.

Compared with other 4-aminonaphthalimide derivatives that are insensitive to pH, the N–H of ENNA is integrated in a large conjugated ring system. As shown in Fig. 2a, the electron-withdrawing inductive effects of the imide moiety and triazole moiety in this ring system weaken the N–H bond. On the other hand, the ENNA anion (base form) can be stabilized by resonance delocalization of the negative charge on to the whole conjugated system, which can be proved by the considerable upfield shift of the ^{1}H NMR signals of all the aromatic protons (H-(a)–(d) and (f)) (Fig. 2b). Both of the above reasons cause the lower pK_a of this fluorophore than that of other 4-aminonaphthalimide derivatives. The negatively charged base form of ENNA has higher electron donor strength than its neutral acid form, which enhances the extent of ICT and results in the red-shifted absorption and emission of the basic form (Fig. 1).

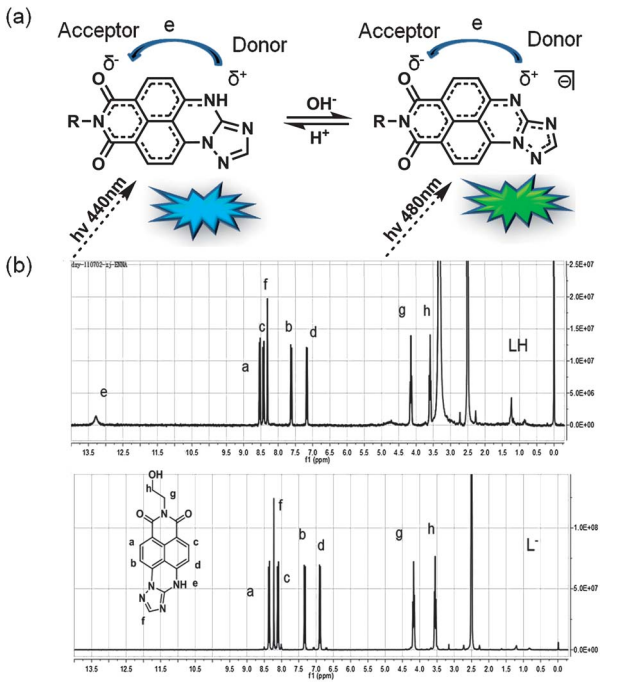

Fig. 2 (a) Proposed sensing process of probe ENNA and (b) ^{1}H NMR spectra taken in DMSO-d_6 without (top) and with (bottom) NaOH.

Stability of ENNA

The stability of ENNA was tested by the time scan of its fluorescence intensity in 20 mM HEPES buffer at pH 5.85, 6.49 and 7.47 respectively under a constant 480 nm excitation over 1 h. The fluorescence intensities of ENNA at different pH remained stable over the time range tested (Fig. S10†), which indicates that ENNA solution is stable to the mediums, light and air.

pH selectivity of ENNA

For pH measurement in biological samples, a good probe should not respond to potential interferents. A selectivity experiment was carried out in 20 mM HEPES containing different metal ions, proteins, and bioactive small molecules, respectively. As shown in Fig. 3, no significant change of the fluorescence intensities was observed at pH 5.33 (Ex/Em: 440/480 nm), pH 6.25 (Ex/Em: 455/510 nm) and pH 7.67 (Ex/Em: 480/510 nm) in the presence of these additives, respectively, indicating that ENNA is highly selective to pH.

Design, synthesis and fluorescence properties of the probe for cellular pH measurement

The above characteristics of this fluorophore make it hold good potential for ratiometric measurement of cellular pH. However, maybe due to the good water-solubility of ENNA and ANNA, both of them exhibit poor cell permeability. In order to increase

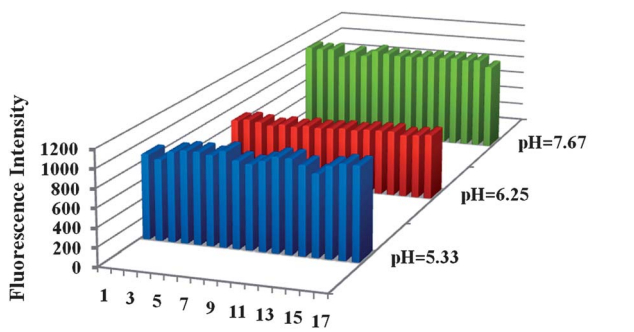

Fig. 3 Fluorescence intensities of 1.0 μM ENNA in 20 mM HEPES buffer at pH 5.33, 6.25, 7.67 in the presence of common metal ions and bioactive small molecules. (1) Blank; (2) Na^+ (100 mM); (3) K^+ (100 mM); (4) Mg^{2+} (0.5 mM); (5) Ca^{2+} (0.5 mM); (6) Zn^{2+} (0.5 mM); (7) Fe^{2+} (0.5 mM); (8) Fe^{3+} (0.5 mM); (9) Hg^{2+} (0.5 mM); (10) glucose (150 μM); (11) D-levulose (150 μM); (12) D-ribose (150 μM); (13) arginine (150 μM); (14) lysine (150 μM); (15) tyrosine (150 μM); (16) tryptophan (150 μM) and (17) bovine serum albumin (150 μM).

the cell permeability of this fluorophore, we have to increase the hydrophobicity by introducing hydrophobic groups.

Usually, substitution at the 9-position (imide N atom) of naphthalimides does not affect their fluorescence properties.[13] The pH response of ENNA and ANNA has been proved to come from the reversible deprotonation of N–H in the heterocycle-fused-naphthalimide ring system. Therefore, we designed a new probe (HNNA) for cellular pH measurement by substitution with a hexadecyl at N-9 of naphthalimide. The long chain substituent can rapidly insert into the bilayer membranes of cells and increase the cell permeability of this fluorophore by the flip–flop mechanism.[14] The synthesized HNNA did not exhibit fluorescence in water and phosphate buffered saline (PBS) because of its low solubility, but exhibited strong fluorescence in ethanol and in surfactant solutions (CTAB, SDS and Triton X-100) (see Fig. S11, ESI†), which suggests that HNNA may locate on the membrane structure of cells. The absorption and emission spectra of HNNA in acidic and basic ethanol showed similar features to those in acidic and basic aqueous solution (see Fig. S12, ESI†). The low fluorescence of HNNA in aqueous solution would reduce the background signal when used for live cell imaging.

pH imaging for living cells

In order to test whether the HNNA can be used for cellular imaging, it was incubated with HeLa cells at 37 °C for 2 hours in DMEM medium. Prior to imaging, cells were washed with PBS (pH 7.4) three times. Fluorescence images were acquired on a laser-scanning confocal microscope (Olympus) with a blue channel (Ex: 405 nm, Em: 425–475 nm) and green channel (Ex: 488 nm, Em: 500–600 nm). As shown in Fig. 4, the fluorescence from both channels could be observed in the cells. HNNA was found to locate on/in the cell membrane, cytoplasm and nuclear membrane, but did not appear in the nucleus. When cells were maintained in PBS (pH 7.4), the green fluorescence in most areas was brighter than the blue fluorescence, but the overlay image clearly showed some blue areas (Fig. 4a), which may suggest the different pH distribution in the cells. When replacing the PBS buffer (pH 7.4) with a low pH, high K^+ HEPES-buffered solution (pH 5.5) and immediately imaging, the green fluorescence on the cell membrane (pointed out by arrows) almost disappeared and the blue fluorescence on the cell membrane increased (Fig. 4b). Both blue and green fluorescence inside the cells did not show significant changes in the first minute after the addition of the low pH buffer (Fig. 4b). The overlay image exhibited significant colour difference between the cell membrane and nuclear membrane (Fig. 4b), which clearly illustrates the pH difference between extracellular and intracellular regions. A dividing cell was clearly observed as two nuclei present in one cell membrane. However, a few minutes after changing the buffer, the green fluorescence in the cells also disappeared (Fig. S13†); this may be due to the pH change inside the cells caused by the low pH high K^+ solution. This set of results suggests the rapid pH response of HNNA in cells.

In order to test the ratiometric fluorescence response of HNNA in cells, MCF-7 cells were firstly incubated with HNNA (4 μM) in DMEM medium for two hours at 37 °C. After removing the medium, cells were treated with nigericin (5 μg mL^{-1}) in high K^+ HEPES-buffered solution at different pH for a further 10 min at 37 °C. Nigericin is a potassium ionophore that allows for the rapid equilibration of pH across biological membranes.[15] As shown in Fig. 5a, at pH 6.36 or lower pH, only the blue channel exhibited fluorescence. With the pH increasing, green fluorescence increased and blue fluorescence decreased gradually. The curve of fluorescence ratio (F_{green}/F_{blue}) *versus* pH was obtained in the pH range of 6.4–8.1 (Fig. 5b), and it can be observed that a small pH change caused a significant change of fluorescence ratio. Based on this ratiometric fluorescence curve, the average pH value of the untreated MCF-7 cells was determined to be

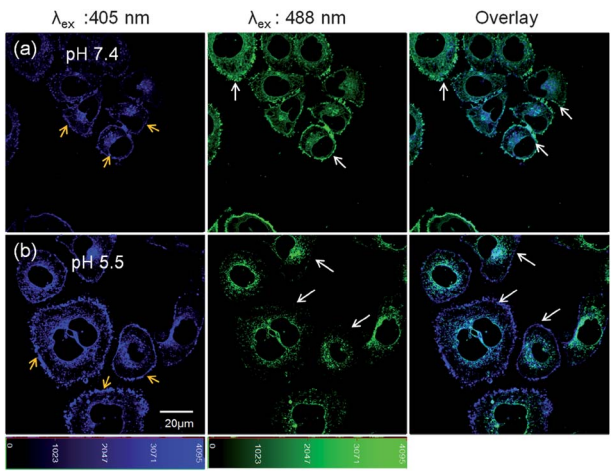

Fig. 4 The confocal images of HeLa cells. (a) Cells maintained in PBS (pH 7.4) and (b) cells in high K^+ HEPES buffer (pH 5.5), collected immediately after changing the buffer. Scale bar: 20 μm, cell membrane was pointed out by arrows.

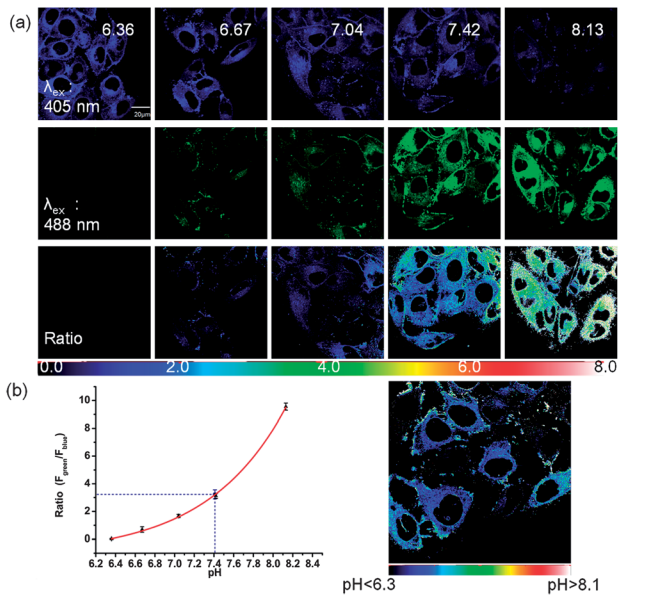

Fig. 5 (a) Confocal fluorescence images of MCF-7 cells incubated in high K^+ HEPES-buffered solution containing ionophores at different pH. (b) pH map (right) calculation for untreated MCF-7 cells based on the calibration curve (left) obtained using ionophores. Scale bar: 20 μm.

7.41 ± 0.06. The ratiometric fluorescence response of HNNA was also observed in HeLa cells, and the intracellular pH value of the HeLa cells was determined to be 7.40 ± 0.02 (see Fig. S14, ESI†).

Usually tumors exhibit a lower extracellular pH (6.2–6.9) than normal tissues (7.2–7.4).[2d,e,3] HNNA was found to locate on the cell surface and inside cells (Fig. 6b). Therefore this ratiometric fluorescent dye would be used to display the pH difference between extracellular and intracellular regions of tumor cells. To mimic the environment of tumor cells, a PBS with a slightly lower pH (6.7) was added to MCF-7 cells that had been incubated with HNNA (4 μM) for two hours at 37 °C. Then the cells were imaged after 5 min at room temperature. In order to enhance the contrast of the images, the blue pseudo colour was changed to magenta. Compared to the images of cells in normal PBS (pH 7.4), the magenta colour on the cell membrane increased after the addition of the low pH PBS (pH 6.7), but no significant change was observed inside the cytoplasm (see Fig. 6a), which resulted in a great colour difference between the cell membrane and cytoplasm in the overlay images. In another experiment, a high K^+ HEPES-buffered solution with lower pH (5.5) was added to the MCF-7 cells and imaged immediately; the images showed that the cell membrane (pointed out by yellow arrows) and the membrane nanotubes between the cells (pointed out by cyan arrows) exhibit a strong magenta color but no green colour, and a significant colour difference was observed between the outer membrane and inner cell in the overlay image (Fig. 6b). These results suggest that HNNA is a good probe candidate for monitoring the pH fluctuations, not only in live cells, but also in the extracellular microenvironment of cancer tissues.

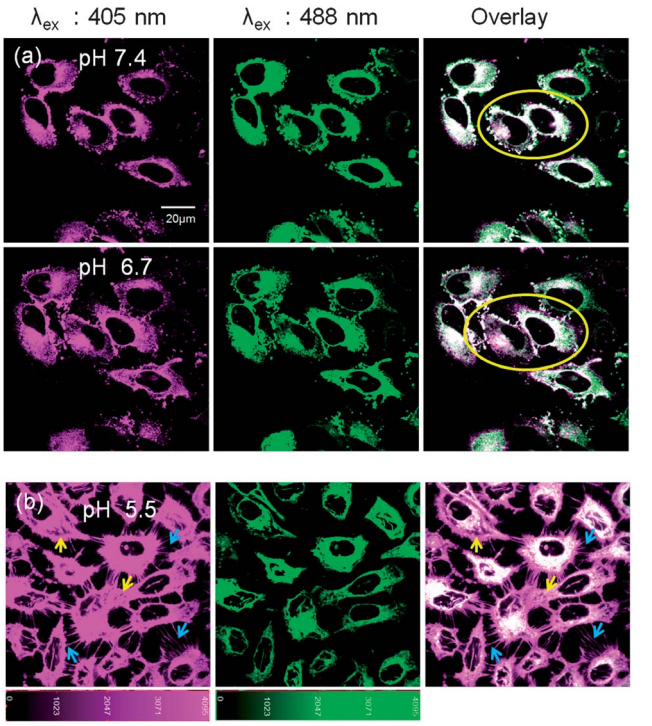

Fig. 6 (a) The confocal images of MCF-7 cells maintained in PBS with pH 7.4 and pH 6.7. (b) The confocal images of MCF-7 cells in high K^+ HEPES-buffer (pH 5.5). Scale bar: 20 μm, cell membranes were pointed out by yellow arrows, membrane nanotubes were pointed out by cyan arrows.

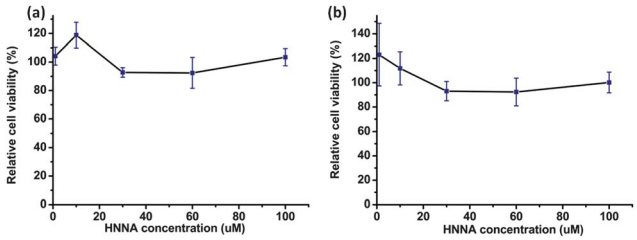

Fig. 7 Cytotoxicity of HNNA at varied concentrations (1 μM, 10 μM, 30 μM, 60 μM, 0.1 mM) on the viability of (a) MCF-7 cells and (b) HeLa cells.

Cytotoxicity assay of HNNA

The cytotoxicity of HNNA was investigated by the standard CCK-8 assay. As shown in Fig. 7, no obvious toxicity toward MCF-7 and HeLa cells was found in the concentration range of 1–100 μM in 24 hours. For pH imaging in cells, 3–5 μM HNNA was enough, suggesting that HNNA can be used to monitor the pH change in living cells over a long period.

Conclusion

In summary, we have described a novel pH sensitive fluorophore that is synthesized by fusing 3-amino-1,2,4-triazole to 4-bromine-1,8-naphthalimides. Three derivatives (ENNA, ANNA and HNNA) with different substituents at the imide N-atom of this fluorophore were synthesized and characterized. The pH response is attributed to the reversible deprotonation of the one and only N–H in the heterocycle-fused naphthalimide structure, with a pK_a of ~6.5. The deprotonation of the N–H enhances the ICT effect of this fluorophore and results in a 30–40 nm red shift of both the absorption and emission spectra. Because of the large conjugated planar structure, this fluorophore possesses high fluorescence quantum yield in both acid and base forms in aqueous solution, which makes it serve as a colorimetric and ratiometric fluorescent probe for pH measurement. This fluorophore has high selectivity to pH, high tolerance to ionic strength, and good stability, which are favourable for cellular pH measurement. A long chain derivative, HNNA, can locate on the membrane structure of the cells, and has been successfully used to map the pH difference in both the extracellular microenvironment and the inner cells by confocal imaging. Because of the easy modification of the imide N-atom, this fluorophore holds great potential for the design of various of ratiometric pH probes for application in biosystems or environmental systems.

Experimental section

Materials and reagents

4-Bromo-1,8-naphthalic anhydride was purchased from Liaoning Liangang Dye Chemical Co. Ltd. 3-Amino-1,2,4-triazole, 6-aminocaproic acid, 1-hexadecylamine and nigericin (sodium salt) were purchased from Alfa Aesar Inc. (Ward Hill, MA). Cell Counting Kit-8 (CCK-8) was bought from Dojindo Molecular

Technologies, Inc. Ethanolamine, ethanol, DMSO and other reagents were purchased from Beijing Chemical Plant, China. All chemical reagents were used without further purification. The stock solutions of probes were prepared in DMSO. Metal ions were prepared with analytical grade nitrate salts or chloride salts. Stock solutions of metal ions and other molecules were prepared in water. Distilled-deionized water was used throughout this work and purified by a UPHW-III-90T upwater purification system (Chengdu, China). All of the titration experiments were performed at room temperature.

Instruments

^{1}H NMR spectra were recorded at 300 MHz, and ^{13}C NMR spectra and DEPT-135° were recorded at 75 MHz on a Brucker AM 300 spectrometer with tetramethylsilane (TMS) as the internal standard. *J* values were given in Hertz. H, H-COSY, NOESY and HSQC were measured on a Brucker AM 600 spectrometer. Low resolution mass spectra (MS) were recorded on a LC-MS 2010A (Shimadzu) instrument using standard conditions. High-resolution MS were obtained on a Bruker Daltonics Flex-Analysis. UV-visible absorption spectra were recorded on a Hitachi U-2550 UV/vis spectrophotometer (Kyoto, Japan). Fluorescence emission spectra were recorded on a Hitachi F-4600 fluorescence spectrofluorometer (Kyoto, Japan) with the excitation and emission slit widths set at 2.5 nm.

Optical measurements

The absorption and fluorescence spectra were recorded in HEPES buffer in a 1.0 cm quartz cuvette. Buffers with different pH were prepared by adding appropriate volumes of 0.2 M NaOH solution or 0.2 M HCl solution to 10 mL of the 20 mM HEPES solution. The fluorescence quantum yield, reversibility, stability and selectivity were measured in HEPES buffer. For UV-vis spectra measurement, 4–5 μL of stock solutions (10 mM) of ENNA or ANNA were diluted in 1 mL of HEPES buffer (at different pH). For emission spectra measurements, 1 μL of stock solutions (1 mM) of ENNA or ANNA were diluted in 1 mL of HEPES (at different pH). The fluorescence emission spectra were collected with excitation at the isoabsorptive point 455 nm. To maintain an ionic strength as the physiological environment, all performances were carried out in the presence of 150 mM NaCl.

Determination of pK_a

The ground-state pK_a values of ENNA and ANNA were determined by collecting their absorption spectra from 350 nm to 550 nm in HEPES buffers (containing 150 mM NaCl) with different pH. The absorbance at 480 nm was plotted *versus* pH value of buffered solution; the data were fit to a Growth/Sigmoidal DoseResp curve (see Fig. S8, ESI†). pK_a values were calculated according to the following equation:

$$pK_a = pH + \log[(A_{HB} - A)/(A - A_B^-)].$$

where, A_{HB}, A and A_B^- represent the absorbance of absolute acid form, the absorbance at the pH chosen and the absorbance of absolute base form respectively.

Confocal imaging

MCF-7 (hormone-dependent breast cancer) and HeLa (cervical adenocarcinoma) cells were purchased from Cell Resource Center of Shanghai Institute for Biological Sciences (Chinese Academy of Sciences, Shanghai, China), and incubated in Dulbecco's Modified Eagle Medium (DMEM, Gibco) supplemented with 10% fetal bovine serum (FBS, Gibco) and 1% penicillin/streptomycin (Hyclone). Cells were cultured in a humidified incubator at 37 °C with 5% CO_2. Cells were imaged under an OLYMPUS FV1000-IX81 confocal microscope (Olympus Corporation, Japan). Fluorescent images (512 × 512 pixels) were observed using a 100× objective lens and the images were processed using the Olympus FV10-ASW 1.6 viewer software. The excitation wavelengths were 405 nm and 488 nm. Fluorescence signals were collected from 425–475 nm in channel I and 500–600 nm in channel II. Ratio data of the images were processed using Image-Pro Plus software.

Cells were seeded in a 35 mm × 12 mm style cell culture dish (*Φ*20 mm glass bottom) and cultured for 24 h. After removing the medium, cells were incubated with 1 mL of fresh medium containing HNNA (4 μM) for 2 h. Prior to imaging, cells were washed with PBS (pH 7.4) three times, and then treated with nigericin (5 μg mL^{-1}) in 1 mL of high K^+ HEPES-buffered solution (different pH) for 10 min. The high K^+ HEPES-buffered solution contained 125 mM KCl, 20 mM NaCl, 0.5 mM $CaCl_2$, 0.5 mM $MgCl_2$, 5 mM glucose and 20 mM HEPES. The different pH was adjusted by adding 0.2 M NaOH. PBS were prepared with 137 mM NaCl, 2.7 mM KCl, 10 mM Na_2HPO_4, and 2 mM K_2HPO_4.

Cytotoxicity assay

MCF-7 and HeLa cells were seeded in 96-well plates (5 × 10^3 cells per well) and grown for 8 h. Then different concentrations of HNNA (100 μM, 60 μM, 30 μM, 10 μM, 1 μM) were added to the cells and they were further incubated for 24 h. Then the medium was replaced with 100 μL of fresh medium containing 10 μL of CCK-8 reagent (without FBS and penicillin/streptomycin). After incubation at 37 °C/5% CO_2 for 1 h, the absorbance at 450 nm was measured on a SpectraMax M5 (Molecular Devices, CA, USA). The cell viability rate (VR) was calculated according to the equation: $VR = (A - A_0)/(A_S - A_0) \times 100\%$, where A is the absorbance of the experimental group, A_S is the absorbance of the control group and A_0 is the absorbance of the blank group (no cells).

Synthesis of compound 1a, *N*-hydroxyethyl-4-bromine-1,8-naphthalimide

2.0 g (7.22 mmol) 4-bromine-1,8-naphthalic anhydride was dissolved in ethanol (160 mL) and heated to reflux. Then 440 μL of ethanolamine (7.3 mmol) was added to the mixture slowly after the temperature was cooled down to 50 °C. The resulting mixture was heated to reflux with stirring for 1 h. The reaction was over when the solution became clear. When the solution was cooled to room temperature, a precipitate emerged. The precipitate was collected by vacuum filtration, and then washed

with water and ethanol three times, respectively, and finally dried by vacuum (yield 90%).

^{1}H NMR ($CDCl_3$, 300 MHz) δ (ppm): 8.65 (d, $J = 9.0$ Hz, 1H), 8.57 (d, $J = 9.0$ Hz, 1H), 8.40 (d, $J = 9.0$ Hz, 1H), 8.03 (d, $J = 9.0$ Hz, 1H), 7.84 (t, $J = 7.5$ Hz, 1H) 4.44 (t, $J = 6.0$ Hz, 2H), 3.98 (t, $J = 6.0$ Hz, 2H), 2.09 (s, 1H); ^{13}C NMR ($CDCl_3$, 75 MHz) δ (ppm): 162.9, 162.9, 132.5, 131.5, 131.3, 130.8, 129.7, 128.9, 128.7, 128.2, 122.8, 122.0, 57.7, 41.9; MS (ESI): m/z 320.1 $(M + H)^+$.

Synthesis of compound 2a (ENNA)

430 mg (1.3 mmol) compound **1a** *N*-hydroxyethyl-4-bromime-1,8-naphthalimide, 200 mg (2.4 mmol) 3-amino-1,2,4-triazole and 120 mg (3 mmol) NaOH were dissolved in DMSO (8 mL). The resulting mixture was heated to 150 °C for 12 h with stirring under an atmosphere of nitrogen. After cooling to room temperature, the solution was evaporated under reduced pressure. The residue was purified by column chromatography using silica-gel (100–200 mesh) and 8% methanol in dichloromethane as eluent to give a salmon pink solid compound (128 mg, 30.7%).

^{1}H NMR (DMSO-d_6, 300 MHz) δ (ppm): 13.28 (s, 1H), 8.54 (d, $J = 9$ Hz, 1H), 8.43 (d, $J = 9$ Hz, 1H), 8.31 (s, 1H), 7.62 (d, $J = 6$ Hz, 1H), 7.17 (d, $J = 9$ Hz, 1H), 4.15 (t, $J = 6$ Hz, 2H), 3.59 (t, $J = 7.5$ Hz, 2H); ^{1}H NMR (DMSO-d_6 + NaOH solid, 300 MHz) δ (ppm): 8.37 (d, $J = 9$ Hz, 1H), 8.22 (s, 1H), 8.11 (d, $J = 9$ Hz, 1H), 7.33 (d, $J = 6$ Hz, 1H), 6.89 (d, $J = 9$ Hz, 1H), 4.18 (t, $J = 7.5$ Hz, 2H), 3.55 (t, $J = 7.5$ Hz, 2H); ^{13}C NMR (DMSO-d_6 + NaOH solid, 75 MHz) δ (ppm): 163.2, 162.7, 155.6, 154.6, 154.3, 139.7, 133.7, 132.7, 132.2, 113.7, 113.3, 111.3, 103.3, 101.5, 58.2, 41.4; MS (ESI): m/z 320.1 $(M - H)^-$; HRMS (ESI): m/z calcd for $C_{16}H_{10}N_5O_3$ $(M - H)^-$ 320.078903, found, 320.078494.

The synthesis and characterization of other compounds can be found in the ESI.†

Acknowledgements

We gratefully acknowledge the financial support from Grant 973 Program (2011CB935800 and 2011CB911000) and NSF of China (21075124).

Notes and references

1 J. Y. Han and K. Burgess, *Chem. Rev.*, 2010, **110**, 2709–2728.
2 (*a*) P. Breedveld, D. Pluim, G. Cipriani, F. Dahlhaus, M. A. van Eijndhoven, C. J. de Wolf and A. Kuil, *et al.*, *Mol. Pharmacol.*, 2007, **71**, 240–249; (*b*) L. Li, Y. Y. Sham, Z. Bikadi and W. F. Elmquist, *Drug Metab. Dispos.*, 2011, **39**, 1478–1485; (*c*) X. L. Wu, J. H. Kim, H. Koo, S. M. Bae, H. Shin and M. S. Kim, *et al.*, *Bioconjugate Chem.*, 2010, **21**, 208–213; (*d*) M. Stubbs, P. M. J. McSheehy and J. R. Griffiths, *Mol. Med. Today*, 2000, **6**, 15–19; (*e*) N. Raghun and R. J. Gillies, *Drug Resist. Updates*, 2000, **3**, 39–47.
3 R. K. Paradise, D. A. Lauffenburger and K. J. Van Vliet, *PLoS One*, 2011, **6**(1), e15746.
4 Y. Tian, F. Su, W. Weber, V. Nandakumar, B. R. Shumway and Y. Jin, *et al.*, *Biomaterials*, 2010, **31**(29), 7411–7422.
5 (*a*) T. Doussineau, S. Trupp and G. J. Mohr, *J. Colloid Interface Sci.*, 2009, **339**, 266–270; (*b*) L. Albertazzi, B. Storti, L. Marchetti and F. Beltram, *J. Am. Chem. Soc.*, 2010, **132**, 18158–18167; (*c*) J. Y. Han, A. Loudet, R. Barhoumi, R. C. Burghardt and K. Burgess, *J. Am. Chem. Soc.*, 2009, **131**, 1642–1643; (*d*) T. Doussineau, M. Smaihi and G. J. Mohr, *Adv. Funct. Mater.*, 2009, **19**, 117–122; (*e*) P. S. Song, X. T. Chen, Y. Xiang, L. Huang, Z. J. Zhou, R. R. Wei and A. J. Tong, *J. Mater. Chem.*, 2011, **21**(35), 13470–13475; (*f*) R. Bizzarri, C. Arcangeli, D. Arosio, F. Ricci, P. Faraci, F. Cardarelli and F. Beltram, *Biophys. J.*, 2006, **90**, 3300–3314; (*g*) X. Zhou, F. Su, H. Lu, P. Senechal-Willis, Y. Tian, R. H. Johnson and D. R. Meldrum, *Biomaterials*, 2012, **33**(1), 171–180.
6 (*a*) A. J. Amali, N. H. Awwad, R. K. Rana and D. Patra, *Anal. Chim. Acta*, 2011, **708**, 75–83; (*b*) L. J. de Nooijer, T. Toyofuku, K. Oguri, H. Nomaki and H. Kitazato, *Limnol. Oceanogr.: Methods*, 2008, **6**, 610–618; (*c*) D. Wencel, M. Barczak, P. Borowski and C. McDonagh, *J. Mater. Chem.*, 2012, **22**, 11720–11729; (*d*) Y. X. Lin, T. Y. Wu and A. F. Gmitro, *J. Biomed. Opt.*, 2012, **17**(4), 046004.
7 (*a*) H. S. Peng, J. A. Stolwijk, L.-N. Sun, J. Wegener and O. S. Wolfbeis, *Angew. Chem., Int. Ed.*, 2010, **49**, 4246–4249; (*b*) A. Schulz, J. Wotschadlo, T. Heinze and G. J. Mohr, *J. Mater. Chem.*, 2010, **20**, 1475–1482; (*c*) W. Shi, X. Li and H. Ma, *Angew. Chem., Int. Ed.*, 2012, **51**, 6432–6435.
8 T. Myochin, K. Kiyose, K. Hanaoka, H. Kojima, T. Terai and T. Nagano, *J. Am. Chem. Soc.*, 2011, **133**, 3401–3409.
9 (*a*) I. Grabchev, I. Moneva, V. Bojinov and S. Guittonneau, *J. Mater. Chem.*, 2000, **10**, 1291–1296; (*b*) X. F. Guo, X. H. Qian and L. H. Jia, *J. Am. Chem. Soc.*, 2004, **126**, 2272–2273; (*c*) X. L. Li, Y. J. Lin, Q. Q. Wang, Y. K. Yuan, H. Zhang and X. H. Qian, *Eur. J. Med. Chem.*, 2011, **46**, 1274–1279.
10 (*a*) D. W. Cui, X. H. Qian, F. Y. Liu and R. Zhang, *Org. Lett.*, 2004, **6**, 2757–2760; (*b*) N. I. Georgiev, V. B. Bojinov and P. S. Nikolov, *Dyes Pigm.*, 2011, **88**, 350–357; (*c*) X. Wan, D. Wang and S. Liu, *Langmuir*, 2010, **26**, 15574–15579.
11 (*a*) N. Boens, W. Qin, N. Basaric, A. Orte, E. M. Talavera and J. M. Alvarez-Pez, *J. Phys. Chem. A*, 2006, **110**, 9334–9343; (*b*) B. M. Weidgans, C. Krause, I. Klimant and O. S. Wolfbeis, *Analyst*, 2004, **129**, 645–650.
12 V. Wintgens, P. Valat, J. Kossanyi, L. Biczok, A. Demeter and T. Berces, *J. Chem. Soc., Faraday Trans.*, 1994, **90**, 411–421.
13 (*a*) I. Grabtchev and T. Philipova, *Dyes Pigm.*, 1995, **27**, 321–325; (*b*) I. Grabtchev, T. Konstantinov, S. Guittonneau and P. Meallier, *Dyes Pigm.*, 1997, **35**, 361–366; (*c*) I. Grabtchev, T. Philipova, P. Meallier and S. Guittonneau, *Dyes Pigm.*, 1996, **31**, 31–34; (*d*) B. May, X. Poteau, D. W. Yuan and R. G. Brown, *Dyes Pigm.*, 1999, **42**, 79–84.
14 F. Kamp, W. Guo, R. Souto, P. F. Pilch, B. E. Corkey and J. A. Hamilton, *J. Biol. Chem.*, 2003, **278**, 7988–7995.
15 (*a*) J. A. Thomas, R. N. Buchsbaum, A. Zimniak and E. Racker, *Biochemistry*, 1979, **18**, 2210; (*b*) J. Llopis, J. M. McCaffery, A. Miyawaki, M. G. Farquhar and R. Y. Tsien, *Proc. Natl. Acad. Sci. U. S. A.*, 1998, **95**, 6803; (*c*) M. Tafani, J. A. Cohn, N. O. Karpinich, R. J. Rothman, M. A. Russo and J. L. Farber, *J. Biol. Chem.*, 2002, **277**, 49569–49576.